Active Internal Waters in the Bacteriorhodopsin Photocycle. A Comparative Study of the L and M Intermediates at Room and Cryogenic Temperatures by Infrared Spectroscopy[†]

Víctor A. Lórenz-Fonfría, Yuji Furutani, and Hideki Kandori*

Department of Materials Science and Engineering, Nagoya Institute of Technology, Showa-ku, Nagoya 466-8555, Japan

Received December 8, 2007; Revised Manuscript Received February 4, 2008

ABSTRACT: We present time-resolved room-temperature infrared difference spectra for the bacteriorhodopsin (bR) photocycle at 8 cm^{-1} spectral and 5 μs temporal resolution, from 4000 to 800 cm^{-1}. An *in situ* hydration method allowed for a controlled and stable sample hydration (92% relative humidity), largely improving the quality of the data without affecting the functionality of bR. Experiments in both $H_2{}^{16}O$ and $H_2{}^{18}O$ were conducted to assign bands to internal water molecules. Room-temperature difference spectra of the L and M intermediates minus the bR ground state (L-BR and M-BR, respectively) were comprehensively compared with their low-temperature counterparts. The room-temperature M-BR spectrum was almost identical to that obtained at 230 K, except for a continuum band. The continuum band contains water vibrations from this spectral comparison between $H_2{}^{16}O$ and $H_2{}^{18}O$, and no continuum band at 230 K suggests that the protein/solvent dynamics are insufficient for deprotonation of the water cluster. On the other hand, an intense positive broadband in the low-temperature L-BR spectrum (170 K) assigned to the formation of a water cavity in the cytoplasmic domain is absent at room temperature. This water cavity, proposed to be an essential feature for the formation of L, seems now to be a low-temperature artifact caused by restricted protein dynamics at 170 K. The observed differences between low- and room-temperature FTIR spectra are further discussed in light of previously reported dynamic transitions in bR. Finally, we show that the kinetics of the transient heat relaxation of bR after photoexcitation proceeds as a thermal diffusion process, uncorrelated with the photocycle itself.

Bacteriorhodopsin (bR),[1] a light-driven proton pump in *Halobacterium salinarum*, is the best studied molecular pump (*1–3*). Bacteriorhodopsin contains all-*trans*-retinal as the chromophore that binds covalently to Lys216 through a protonated Schiff base (SB). Upon light absorption, photoisomerization takes place from the all-*trans* to 13-*cis* form in less than one picosecond, followed by a cyclic reaction that comprises a series of intermediates, designated as the K, L, M, N, and O states, back to the bR ground state (BR). During the bR photocycle, the primary proton transfer takes place in the L to M transition. A proton is transferred from the protonated SB to Asp85, together with the apparently simultaneous release of a proton from the so-called proton release group (PRG) to the extracellular side. Further proton transfers take place in the M to N, N to O, and O to BR transition (accompanied by other protein and retinal structural changes), leading to a net proton transport from the cytoplasmic to the extracellular side, and the recovery of the bR ground state.

Bacteriorhodopsin has become a paradigm not only for proton transfers and transport but also for the active role of internal water molecules in protein function. Low-temperature FTIR difference spectroscopy showed changes in the O−H stretching of some internal water molecules, reflecting changes in their H-bond strength during different steps of the photocycle (*4, 5*). More recently, X-ray crystallographic structures of cryo-cooled bR ground-state crystals have revealed the presence of more than 20 ordered water molecules, nearly 10 of them along the putative proton pathway (*6, 7*). Similar X-ray crystallographic studies of the photocycle intermediates from the wild type and some mutants show rearrangements and relocations for some of the internal water molecules during the photocycle (*8–10*), although with some discrepancies between different groups (*11*).

It should be noted that low-temperature studies of internal water molecules in bR are based on the assumption that positions and properties of water molecules are similar at room and low temperature. It is generally accepted that bR intermediates trapped at low temperatures should display a protein structure and a retinal conformation essentially equivalent to those of their room-temperature counterparts (*11*), but can such argument be applied to internal water molecules? Even if the time-averaged bR protein structures

[†] This work was supported by grants from Japanese Ministry of Education, Culture, Sports, Science, and Technology to H.K. (15076202 and 19370067) and by a Research Fellowship for Foreign Researchers from the Japan Society for the Promotion of Science to V.A.L.-F.

* To whom correspondence should be addressed. Phone and fax: 81-52-735-5207. E-mail: kandori@nitech.ac.jp.

[1] Abbreviations: bR, bacteriorhodopsin; BR, light-adapted bR ground state; SB, Schiff base; PRG, proton release group; FTIR, Fourier transform infrared spectroscopy; HOOP, hydrogen out-of-plane bending vibration.

10.1021/bi7024063 CCC: $40.75 © 2008 American Chemical Society
Published on Web 03/06/2008

and retinal conformations for the different intermediates are truly conserved at low temperatures, protein dynamical fluctuations are certainly attenuated as the temperate decreases (*12*). Two dynamic transitions inhibited by low temperatures are present in bR. One transition at ~250 K corresponds to the inhibition of some fast−small and slow−large motions (in the scale of neutron diffraction), with the slow−large motions depending on the protein−"hydrating water" interaction (*13–16*), while another transition at ~170 K corresponds to inhibition of some slow−large motions, independent of the sample hydration level (*15, 16*). Due to their potential mobility, it seems perfectly conceivable that internal waters could be significantly affected in their interactions, or even in their location, by the reduced protein and/or solvent dynamics when the bR ground state and the bR intermediates are studied at low temperatures.

To gain insight into these problems, it is important to compare the O−H stretching region for low- and room-temperature intermediates. This is challenging given the large and variable background absorbance of bulk water when films are hydrated at room temperature. As a consequence, only the regions below ~3000 cm^{-1} (*17–19*), or above 3500 cm^{-1} (*20*), have been presented and analyzed in some detail until now. Even though in these regions the bulk water absorbance is still relatively low, the spectroscopic data presented so far have been discouragingly noisy and/or embedded in large baselines from the transiently heated bulk water. The problem of the bulk water absorbance at room temperature was solved in this work by controlling *in situ* the hydration level of purple membrane films, following an approach recently introduced by Noguchi and Sugiura (*21*). This allowed us for the first time to obtain high-quality time-resolved room-temperature FTIR spectra of the bR photocycle, including the O−H stretching region, and a reliable investigation of differences in internal waters molecules between room- and low-temperature spectra for the L and M intermediates with respect to the bR ground state (L-BR and M-BR, respectively).

MATERIALS AND METHODS

Time-Resolved Step-Scan FTIR Spectroscopy. Approximately 60 μL of bR in the purple membranes (2 mM KP_i at pH 7.0) was dried over a BaF_2 window with a diameter of 2.5 mm. The dry film was hydrated with the saturated vapor phase of five drops (5 μL) of a glycerol/water mixture, ranging from 50 to 10% (glycerol volume to total volume). It was closed with a second window using a silicone O-ring and placed in a sample holder. Note that the film was never in direct contact with the glycerol/water mixture, being hydrated from the vapor phase. The conditions selected to conduct the experiments were 30% glycerol, which corresponds to a relative humidity of ~92% (*21*). Using the integrated extinction coefficient for water between 3700 and 2900 cm^{-1} (~39200 M^{-1} cm^{-2}) (*22*), and for the peptide bonds between 1700 and 1480 cm^{-1} (~32500 M^{-1} cm^{-2}) (*23*), we estimated the presence of ~800 water molecules per bR monomer (0.55 g of H_2O/g of bR), similar to previous estimates at this relative humidity (*13*). Typical bands for all the intermediates (K, L, M, N, and O) were observed (see Results), pointing to a fully functional photocycle, although with slower ground-state recovery, in agreement with previous studies on the effect of the hydration level on the bR photocycle (*24*).

Time-resolved step-scan experiments were performed in an optics compartment-evacuated Bruker IFS 66v/S FTIR spectrometer placed over a vibration isolation table (TDI-1510LA from Herz). A bR film hydrated with the vapor phase of a glycerol/water mixture (with either $H_2{}^{16}O$ or $H_2{}^{18}O$) was placed in a sample holder connected to a circulating thermostatic bath set to 20.0 °C. The sample window normal was only slightly tilted with respect to the IR beam (~5°), forming a roughly 65° angle with the excitation laser beam. Photoreaction was induced at 1480 different mirror retardations by a 10 ns, ~1.5 mJ/cm^2 per pulse, 532 nm Nd:YAG laser (Quanta-Ray INDI, Spectra-Physics). Before data were acquired, the samples were light-adapted with ~2 min of 10 Hz laser pulses. The DC detector signal was sampled every 5 μs by a 200 KHz 16 bits ADC, and data acquisition was initiated 500 μs before the sample was excited at a 10 Hz repetition rate by the laser, and finished ~13 ms later. Synchronization of data acquisition and laser triggering was performed using a delay pulse generator (DG535; Stanford Research Systems). For signal-to-noise improvement, eight photoreactions were averaged at each mirror position (acquisition time of ~20 min) and 20–25 time-resolved single-beam spectra were recorded and averaged for a given sample (experiment length of ~9 h). Single-beam spectra recorded before laser excitation were averaged and used to transform the single-beam spectra to absorbance spectra. For further signal-to-noise improvement, six such experiments were averaged for $H_2{}^{16}O$, and two for $H_2{}^{18}O$, using a fresh film each time. Control experiments characterizing the ground-state recovery as a function of the hydration were performed at 4 Hz, sampling every 20 μs, and using an optical filter (LP-5100, Spectrogon) to allow for the longer acquisition time before the ADC ran out of memory (up to 140 ms).

Low-Temperature FTIR Spectroscopy. Low-temperature spectra of K-BR (77 K, pH 7), L-BR (170 K, pH 7), M-BR (230 K, pH 10 and 7), and N-BR (273 K, pH 10) in $H_2{}^{16}O$ and $H_2{}^{18}O$ were obtained at 2 cm^{-1} from light-adapted hydrated films, as described and partially presented elsewhere (*4*).

Data Postprocessing. Time-resolved room-temperature difference spectra were averaged quasi-logarithmically to a maximum of 10 spectra per decade. Low-temperature spectra were mathematically converted from 2 to 8 cm^{-1} by deapodization/apodization in the Fourier domain, allowing for a comparison with the room-temperature difference spectra free from instrumental resolution differences. Both room-temperature and low-temperature difference spectra were automatically baseline-corrected, making the absorbance at the 3900 and 2200 cm^{-1} regions as close to zero as possible in the least-squares sense. No further data postprocessing, e.g., SVD or global exponential fitting, was performed to improve the appearance of the data.

Estimation of the Transient Intermediate Fractions. Some of the bands in the IR difference spectra of the bR photocycle are highly or partially selective with respect to some of the bR intermediates and thus can be used to obtain an estimation of the intermediate fractions as a function of time without using any specific kinetic model. The procedure was as follows. The kinetics of accumulation of the K intermediate

was obtained from the area of the retinal HOOP positive band at 984 cm^{-1}, integrated between 993 and 972 cm^{-1} (*25*). For the L intermediate, we used the area of the carboxylic negative band at 1740 cm^{-1} integrated between 1749 and 1731 cm^{-1}, mainly corresponding to Asp96 and partially to Asp115 side chain alterations (*26*). The kinetics of the M intermediate was followed by the area of the appearing carboxylic positive band at 1762.5 cm^{-1} integrated between 1774 and 1754 cm^{-1}, corresponding to Asp85 (*26*). For the N and O intermediates, we used the area of the negative amide I band at ~1670 cm^{-1}, integrated between 1682 and 1659 cm^{-1} (*27*). Given their relatively low level of accumulation and time overlap, no attempts were performed to resolve their individual fractions. The fraction of BR as a function of time was obtained from the area of the negative band at 1253.5 cm^{-1} (*27*), integrated between 1283 and 1239 cm^{-1}. All the areas were calculated using a baseline between the integrated intervals. To obtain the intermediate fractions as a function of time (shown in Figure 3a), the kinetics for the selective intermediate bands were scaled using the following criterion: the sum of all K, L, M, N + O, and BR fractions should be as close as possible to one in the least-squares sense. This criterion could be successfully fulfilled except for the first data point (see Figure 3a, Total trace), likely due to an imperfect synchronization of the sample excitation and the data acquisition. The estimated intermediate fractions from 2.5 μs to 13 ms were globally fitted using five exponentials (final time constants of 4 μs, 80 μs, 300 μs, 3 ms, and 40 ms) using a homemade program running in MATLAB version 7, as described previously (*28*).

RESULTS

Control of the Sample Hydration Level. At room temperature, we control the hydration level of a purple membrane film with the saturated atmosphere of a glycerol/water mixture (see the details in Materials and Methods). Figure 1 shows how the absorbance spectrum of a purple membrane film depends on the glycerol/water mixture used for hydration. The selected condition for carrying out further experiments was 30% glycerol (Figure 1, black line). This condition gives a tolerable bulk water absorbance, which remains constant during one time-resolved step-scan FTIR measurement (~20 min). Furthermore, 30% glycerol gives a relative humidity of ~92% at saturation (*21*), which is considered to be sufficient for the functional photocycle (*24*). The photocycle ground-state recovery kinetics for some hydration conditions is presented in Figure 1 (inset). The bR ground-state recovery slowed as the level of hydration was reduced. At 92% relative humidity (30% glycerol), ~100 ms is required for a 95% bR ground-state recovery. To allow for a more extensive data averaging, further time-resolved step-scan experiments were performed exciting the sample every 100 ms (10 Hz). The possibility of artifacts caused by the potential photoexcitation of the 5% remaining fraction of bR intermediates was ruled out by performing control experiments at 5 Hz photoexcitation, providing indistinguishable time-resolved spectra within the noise level (not shown).

Room-Temperature Time-Resolved FTIR Data. Figure 2 shows eight selected time slices (from 2.5 μs to 5.3 ms) of time-resolved step-scan FTIR experiments for the bR photocycle. The experiments were performed as described in

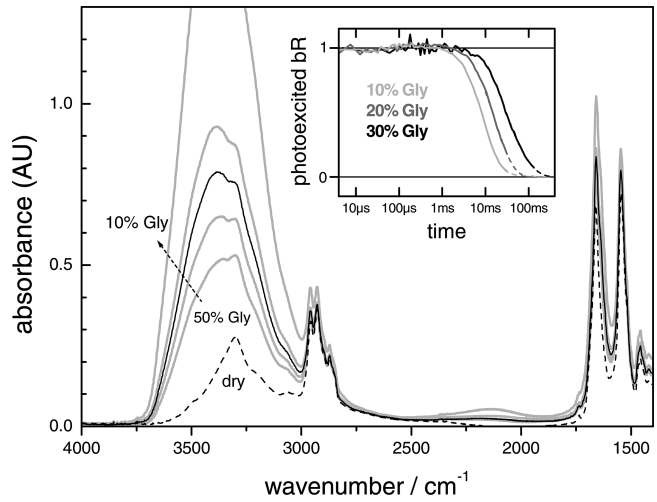

FIGURE 1: Absorbance spectra of a purple membrane film under various hydration conditions: dried (dashed line) and hydrated with the vapor phase of different glycerol/water mixtures (gray lines). The condition selected for conducting further experiments was 30% glycerol (black line). The inset shows the experimental kinetics of the normalized 1253.5 cm^{-1} area in the time-resolved difference spectra of the bR photocycle (see Figure 2, right panel), proportional to the fraction of the photoexcited bR, for different hydration conditions (solid lines). The experimental kinetics were extrapolated by multiexponential fitting to visualize the final signal decay (dashed lines).

Materials and Methods, for a purple membrane film hydrated with the vapor phase of a 30% glycerol/water mixture. Figure 2 (right panel) shows the 1800–900 cm^{-1} region (*29–32*), with bands coming from the retinal, the Schiff base, the protein backbone, and amino acid side chain vibrations of BR (negative) and photointermediates (positive). Detailed information about spectral assignments has been published elsewhere (*16, 33, 34*).

Figure 2 (left panel) shows difference IR spectra for the bR photocycle in the X−H stretching region for several representative time points. Spectra at early times are dominated by an intense and broad bilobed peak. Overlaid with the bilobed peak is a fine structure of positive and negative bands, which becomes evident when the bilobed signal decreases in intensity after 100 μs. The fine structure originates from O−H, N−H, or C−H vibrations of the protein, retinal, and internal waters changing during the photocycle and will be discussed later. Note that even at this reduced hydration level, the bulk water absorbance (shown as a gray pattern-filled spectrum in Figure 2, left panel) is still at least 3 orders of magnitude more intense that any spectral changes related to the photocycle in the X−H region. The intense bilobed peak in the time-resolved data can be effectively reproduced by a temperature-induced difference spectrum of a hydrated purple membrane film (298 K minus 293 K), with a scaling factor corresponding roughly to a 0.3 K temperature increase at 2.5 μs (gray line in the left panel of Figure 2). Taking into the account its intensity and how well the bilobe shape is reproduced by the static temperature-difference spectrum, we conclude that it originates from the transient heat of the bulk water present in the hydrated purple membrane.

Figure 3a shows an estimation of the intermediate fractions as a function of time, obtained from some intermediate-selective bands areas. The procedure is described in detail in Materials and Methods. From Figure 3a, we can conclude

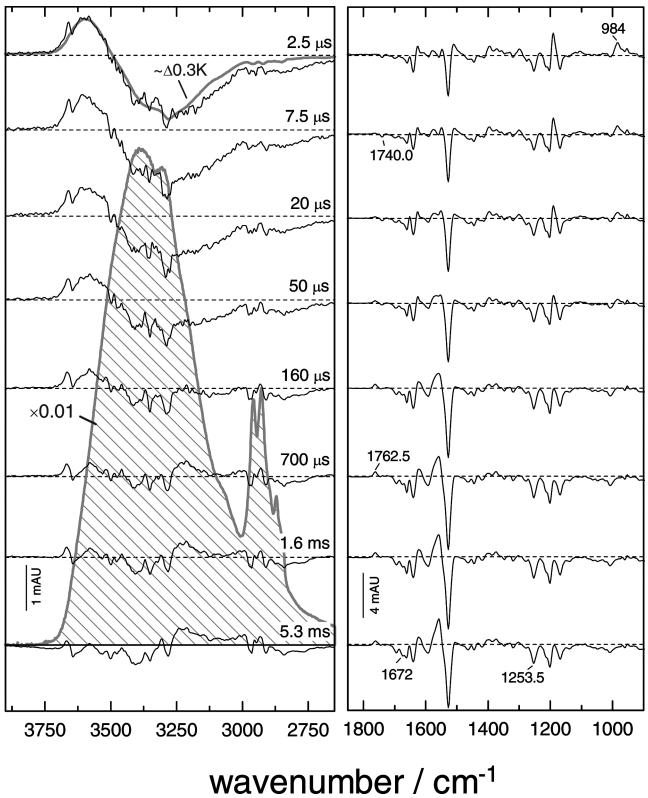

FIGURE 2: Room-temperature (293 K) time-resolved FTIR difference spectra for the bR photocycle at eight selected times from 2.5 μs to 5.3 ms (see the left panel) at neutral pH. Bands used to monitor accumulation of intermediates and ground-state recovery are labeled (see the right panel). The right panel shows the 1850–900 cm^{-1} region. The left panel includes the data from the 3900–2650 cm^{-1} region, which comprises the X−H stretching vibrations. The pattern-filled spectrum corresponds to the background film absorbance in the X−H stretching region (note its different scale). The gray spectrum corresponds to a temperature-induced difference spectrum (298 K minus 293 K) for a hydrated purple membrane film, appropriately scaled to mimic the intense bilobed peak at 2.5 μs.

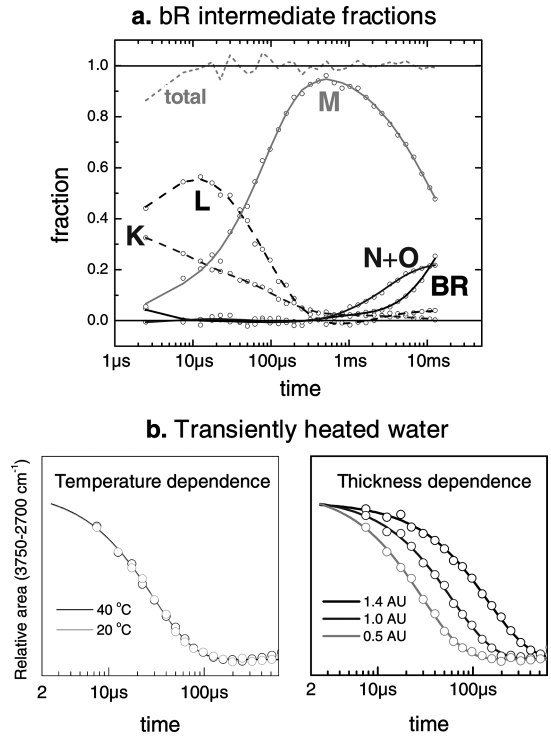

FIGURE 3: (a) Estimated intermediates fractions as a function of time under the experimental conditions used in this study (○). The estimates were obtained as described in Materials and Methods, using the area of some intermediate-selective bands, appropriately scaled for the total fraction being close to one. Due to its low and kinetically similar accumulation, the N and O intermediates were grouped together. The solid and dashed lines correspond to fits provided by global exponential fitting. (b) Relaxation kinetics of the transiently heated water, monitored by the absolute area between 3750 and 2700 cm^{-1} (○), and corresponding monoexponential fits (solid lines). The right panel illustrates the dependence of relaxation on the film thickness (measured by the amide I maximum intensity), with time constants of 30, 60, and 140 μs. The left panel illustrates the independence of relaxation on temperature for a fixed film thickness (amide I of ~0.5 AU).

that under these experimental conditions the level of accumulation of M is very high, with a maximal accumulation fraction of 0.95 at ~500 μs. The level of accumulation of the L intermediate is also substantial, reaching a fraction of 0.55 at ~11 μs. As expected, the times of maximal accumulation are slightly slower than those for well-hydrated films (*35*). The rest of the intermediates showed a lower level of accumulation, at times too early (K) or too late (N and O) to provide reliable features in the X−H stretching region. Therefore, further analyses were limited to the L and M intermediates.

Figure 3b shows the kinetics of the transient heat under different conditions, monitored by the bilobed absolute area. The transient heat emerges in less than 20 ns (*36*), and it is not resolved here. Figure 3b (left panel) shows how the heat relaxation kinetics is not affected by the sample temperature, in contrast to the relaxation steps of the bR photocycle (*37*). Moreover, the heat relaxation kinetics is delayed when the sample thickness, monitored by the amide I intensity, increases (Figure 3b, right panel). These data strongly suggest that the heat released in the primary photoisomerization step dissipates from the sample via a conventional thermal diffusion process, proceeding in a manner that is uncoupled with further steps of the bR photocycle.

Room-Temperature versus Low-Temperature M-BR Spectra. Figure 4 shows a difference spectrum obtained by averaging the time-resolved difference spectra between 500 μs and 2 ms (red line). According to Figure 3a intermediate fraction estimates, it corresponds to almost pure room-temperature M-BR (~90%) with a remaining minor contribution of N-BR (~10%). We also fitted the retinal fingerprint region between 1300 and 1100 cm^{-1} to low-temperature pure M-BR and N-BR difference spectra (not shown), obtaining a comparable estimate: 85% M-BR and 15% N-BR.

Figure 4a compares the room-temperature M-BR spectrum (red line) with the low-temperature M-BR spectrum (blue line), obtained under conditions providing pure M-BR (230 K and pH 10). The agreement in the 1800–800 cm^{-1} region is excellent, including the retinal (1558, 1528, 1201, 1168, 1008, 960, and 952 cm^{-1}), the protein backbone (1694 and 1661 cm^{-1}), and amino acid side chain (1762, 1746, and 1739 cm^{-1}) bands. Small intensity differences in the amide I region and in the 1528 and 1180 cm^{-1} retinal bands could be explained either by the small contribution of N-BR to the room-temperature M-BR spectrum or by differences in the experimental conditions (e.g., temperature, pH, sample tilt, etc.).

For the first time, Figure 4b presents a detailed view of the M-BR spectrum in the 3800–2500 cm^{-1} region, for both

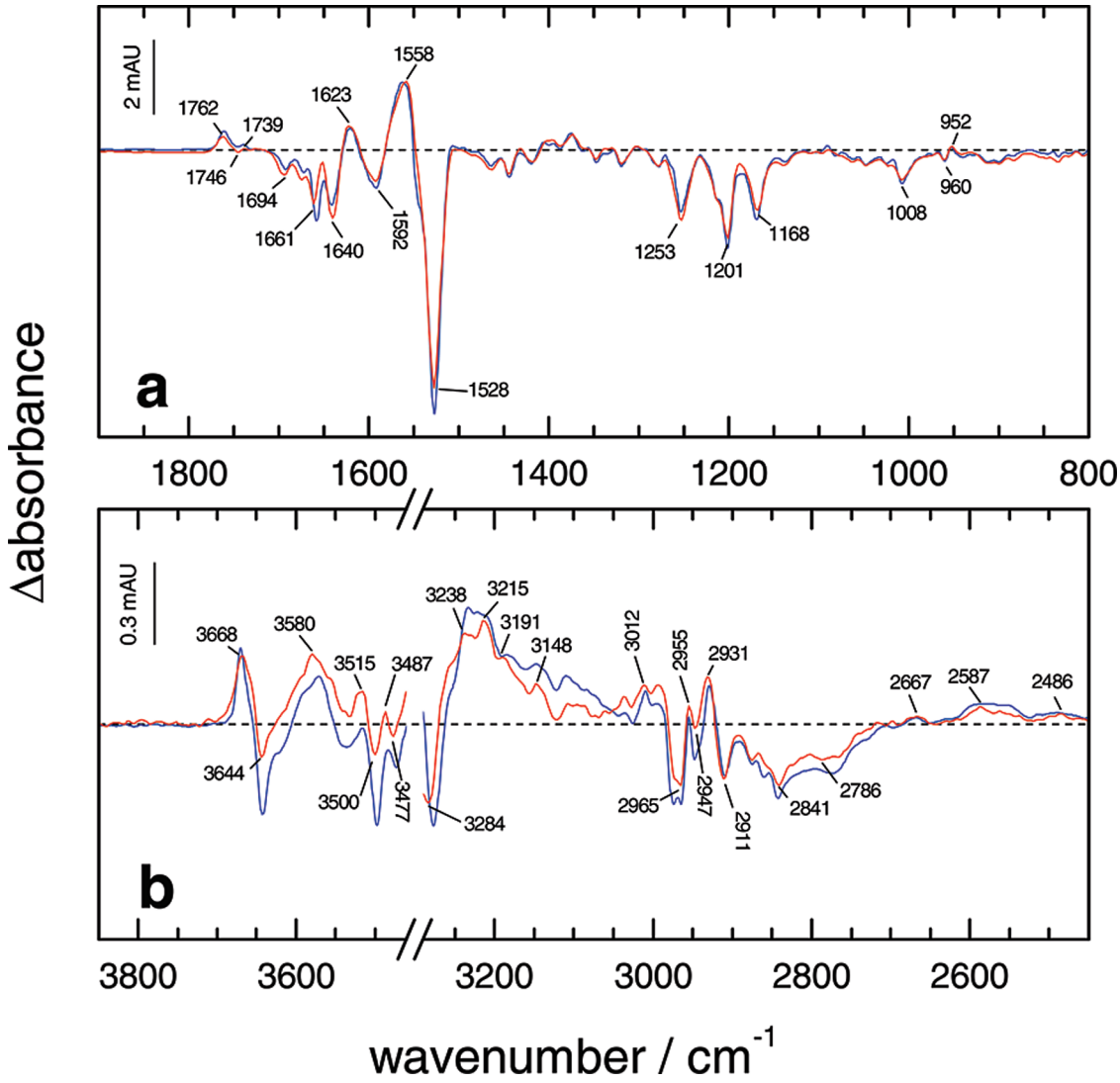

FIGURE 4: Room-temperature (red line) and low-temperature (blue line) M-BR infrared difference spectra. The room-temperature M-BR spectrum was obtained by averaging the time-resolved FTIR spectra in Figure 2 between 500 μs and 2 ms, corresponding to almost pure M-BR with a 10% contribution of N-BR at neutral pH. The low-temperature M-BR spectrum was obtained at 230 K and pH 10, corresponding to pure M-BR, and it was appropriately scaled for a comparison with the room-temperature data: (a) 1900–800 cm^{-1} region and (b) 3850–2650 cm^{-1} region. The 3460–3290 cm^{-1} interval is not displayed, since some features of the low-temperature data may not be reliable due to the high background absorbance.

room-temperature (red line) and low-temperature (blue line) data. Note that the bands in this region are much less intense, with almost 1 order of magnitude difference in the scales between panels a and b. This region corresponds to X−H vibrations changing between M and BR, notably from O−H, N−H, and C−H vibrations from water, protein, retinal, and/or lipids. Only a few of the bands in this region have been assigned, mainly those from weakly H-bonded waters, as well as some bands from amino acid side chains and the backbone amide A (*38–40*). Both room- and low-temperature spectra are reasonably similar, with bands appearing basically at the same wavenumbers. The band intensities and shapes are also comparable, in spite of some differences. This represents further evidence for the similitude of the room-temperature and low-temperature M-BR spectra, this time also from the point of view of the O−H, N−H, and C−H stretching vibrations. Some of the observed minor differences between low- and room-temperature M-BR may be caused by differences in the pH. Indeed, the spectrum of the low-temperature M-BR at pH 7, in spite the possible L-BR contamination, was closer to the room-temperature M-BR (Figure S1 of the Supporting Information).

Internal Water Spectral Changes in M-BR. Figure 5a shows how weakly H-bonded water vibrations change between the bR ground state and the M intermediate at room temperature. Water bands are assigned by their downshift when $H_2{}^{16}O$ (red line) is replaced by $H_2{}^{18}O$ (blue line). The spectral signatures for the weakly H-bonded waters are basically similar to those found at low temperatures (Figure 5b). The spectral differences could be ascribed mostly to effects of pH on the band positions, bandwidths, and/or bandshapes (see Figure S1).

Unlike the situation for the weakly H-bonded water, the O−H stretching of strongly H-bonded water does not give rise to narrow bands, but to relatively broad bands appearing below 3000 cm^{-1}. At low temperatures, no band is observed to shift in $H_2{}^{18}O$ (Figure 5d), suggesting no change in strongly H-bonded waters between M and BR, in agreement with previous studies in D_2O (*5, 41*). Within the noise level, the same conclusion holds for the room-temperature data

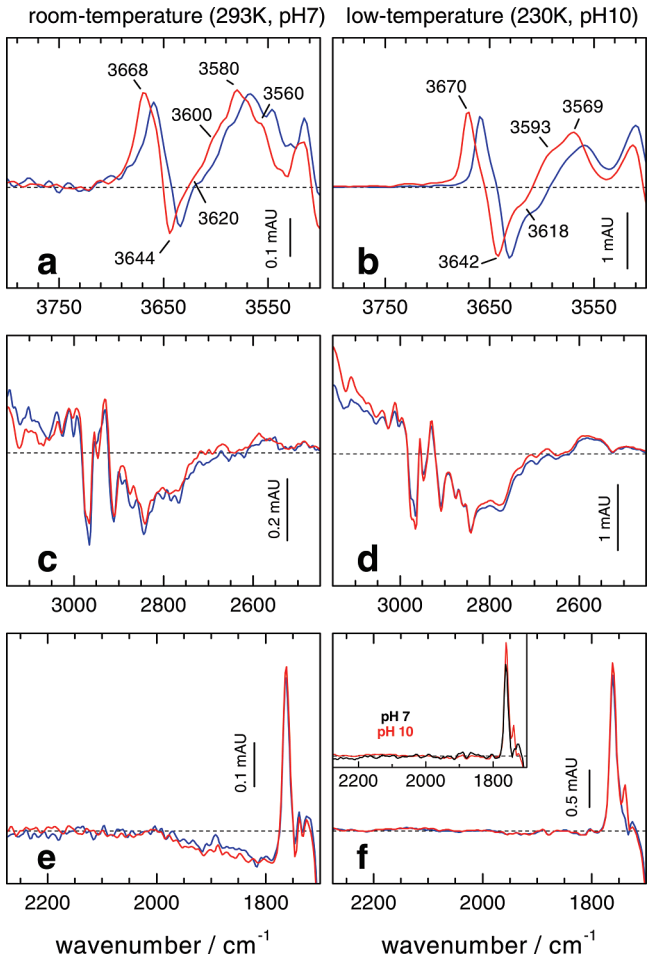

FIGURE 5: Comparison of water regions between the room-temperature (left) and low-temperature (right) M-BR spectra. Bands from water O−H vibrations were assigned and labeled by their isotopic downshift when $H_2{}^{16}O$ (red lines) was substituted by $H_2{}^{18}O$ (blue lines). (a and b) Weakly H-bonded O−H stretching region. (c and d) Strongly H-bonded O−H stretching region. (e and f) Protonated water continuum region. (f, inset). Protonated water continuum region for the low-temperature M-BR at pH 10 (red line) and pH 7 (black line). At pH 7, M-BR is significantly contaminated with L-BR, explaining the lower intensity of the Asp85 carboxylic band.

(Figure 5c). Note again the remarkable spectral similarity between the room- and low-temperature data for the M-BR spectrum. This degree of similarity is even higher when both spectra are measured at the same pH (see Figure S1).

Another spectral signature related to internal water molecules has been reported in the room-temperature bR photocycle: a negative continuum band that can be observed at around 2200–1800 cm^{-1}. The band correlates with the deprotonation of the proton release group, the group releasing a proton to the extracellular side in a manner concomitant with the SB deprotonation, and a protonated water cluster has been proposed as the origin (*18, 42*), though there was no direct evidence of a water signal. The red curve in Figure 5e shows how this negative continuum band is also present in our M-BR spectrum at room temperature (2000–1800 cm^{-1}). Moreover, our data strongly suggest that the continuum band contains a water signal. The blue curve in Figure 5e represents the M-BR spectrum in $H_2{}^{18}O$. While red (H_2O) and blue ($H_2{}^{18}O$) curves coincide with each other at other frequencies (data not shown), there was a clear spectral difference at 2000–1800 cm^{-1}. Such a difference does not look like a typical isotope shift, presumably because of a broad spectral feature, but it was reproducible. From this isotope effect, we concluded that the continuum band contains a water vibration.

Figure 5f shows the same region for the low-temperature M-BR spectrum. In contrast to the room-temperature data, no continuum band is observed at low temperatures, with a completely flat baseline from 2200 to 1800 cm^{-1} in both $H_2{}^{16}O$ and $H_2{}^{18}O$. However, note that the low-temperature M-BR spectrum shown in Figure 5 (and Figure 4) was obtained at pH 10. At this high pH, the proton release could be inhibited (*43*), which could explain the lack of a continuum band at low temperatures. This possibility was ruled out via a comparison of the continuum band region for the low-temperature M-BR at pH 10 and 7 (see the inset of Figure 5f).

Room-Temperature versus Low-Temperature L-BR Spectra. From the room-temperature time-resolved spectra shown in Figure 2, we obtained the room-temperature L-BR spectrum, averaging the data between 5 and 50 μs. According to our estimates from Figure 3a, this provides a spectrum comprising 50% L-BR with significant contributions of K-BR (25%) and M-BR (25%). We also fitted the retinal fingerprint region between 1300 and 1100 cm^{-1} to low-temperature K-BR, L-BR, and M-BR spectra (not shown), providing a close estimate of 60% L-BR, 15% K-BR, and 25% M-BR. As indicated in the inset of Figure 6a, the room-temperature M-BR contribution could be removed from the room-temperature L-BR using the Asp85 band at ~1762 cm^{-1} as a reference for the subtraction process. After this correction, the obtained L-BR spectrum (hereafter, called the room-temperature L-BR spectrum) corresponds mainly to the L-BR spectrum (65–80%) with the remaining contribution being K-BR.

Figure 6 compares room-temperature (red) and low-temperature (blue) L-BR spectra. Low-temperature L-BR was obtained at 170 K and pH 7, corresponding to pure L-BR. Since the room-temperature L-BR contained a substantial contribution of K-BR, Figure 6a also includes (in cyan) a low-temperature L-BR spectrum (70%) with an added low-temperature pure K-BR spectrum (30%). Figure 6a shows the 1800–900 cm^{-1} region. We observe differences between the room-temperature (red) and low-temperature (blue) data, most remarkably in the HOOP region (band at 985 cm^{-1}), but also in other retinal bands, as well as in protein amide bands. Our room-temperature L-BR contribution, as well as the observed differences with low-temperature L-BR, is in agreement with previous reports (*26, 32, 44*). However, when the K-BR contribution is taken into account, the differences in the HOOP region remain, but the retinal fingerprint region (bands at 1252, 1203, 1191, and 1169 cm^{-1}) as well as the retinal C═C bands at 1528 and 1510 cm^{-1} becomes quite similar between the room-temperature (red) and low-temperature (cyan) data. Still, some differences in the 1750–1550 cm^{-1} region persist (mostly at ~1740, 1660, and 1560 cm^{-1}), suggesting small but significant protein structural differences between room and low temperature, mainly in the protein backbone helical changes and Asp96/Asp115 alterations taking place between BR and L.

Figure 6b shows for the first time in detail the 3800–2700 cm^{-1} region for the L-BR intermediate, for both room and low temperature. The room-temperature spectrum (red) is

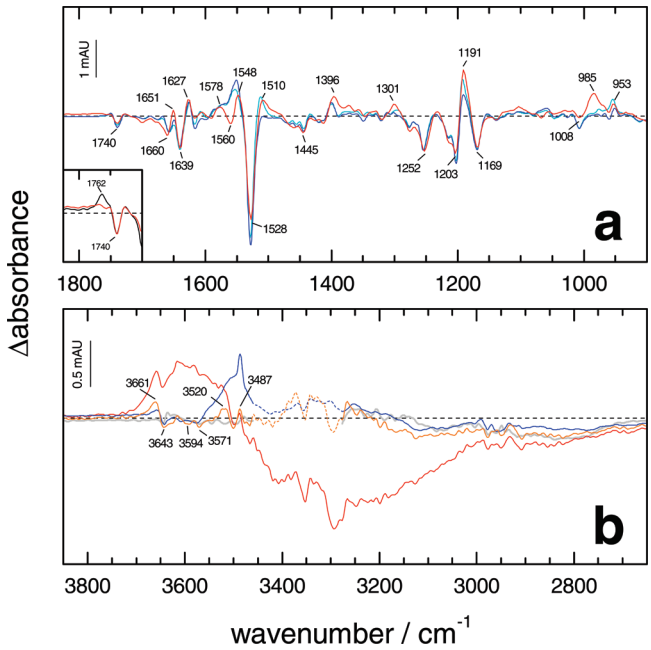

FIGURE 6: (a) Room-temperature IR difference spectrum averaged between 5 and 50 μs, corresponding mainly to L-BR (50%) with K-BR (25%) and M-BR (25%) contributions (black line). The M-BR contribution (manifested by the positive Asp85 band at ~1763 cm^{-1}) was mathematically removed (red line) using the room-temperature M-BR spectrum shown in Figure 4. (a) Room-temperature L-BR, corresponding to 70% L-BR and 30% K-BR (red line), is compared with low-temperature L-BR (blue line), and with low-temperature L-BR with the added low-temperature K-BR spectrum (cyan line), in the 1825–900 cm^{-1} region. (b) The 3850–2650 cm^{-1} region, showing also the room-temperature L-BR corrected for the transient heat (orange line), and the low-temperature K-BR (gray line). The dashed lines correspond to spectral features that may not be reliable due to the high background absorbance.

dominated by the broad bilobed peak assigned to transiently heated water. We subtracted this contribution using the temperature-induced difference spectrum shown in Figure 2 (left panel). The resulting spectrum is colored orange. When it is compared with the low-temperature L-BR spectrum (blue), one can observe a basic agreement between them. Both show a few well-defined bands, and mostly baseline-like contributions. However, between 3550 and 3450 cm^{-1}, an intense broadband clearly present at low temperatures is completely missing at room temperature. As shown below and discussed in the literature, this band originates from some internal waters under weak H-bonding which appear in the cytoplasmic domain when L is formed (*4, 38, 45*).

Internal Water Spectral Changes in L-BR. Figure 7a shows the room-temperature L-BR corrected for the transiently heated water, for both $H_2{}^{16}O$ and $H_2{}^{18}O$. The limited signal-to-noise ratio of the $H_2{}^{18}O$ data allows us to observe only a clear downshift for the 3642 cm^{-1} band, assigned thus to an internal water. Figure 7b shows the same wavenumber interval for low-temperature L-BR. At least three negative and two positive overlapped bands can be assigned to water molecules. When panels a and b of Figure 7 are compared, it is clear that, although the negative bands assigned to water at low temperatures could conceivably be present at room temperature, hidden under the noise, the intense broadband seems to be missed.

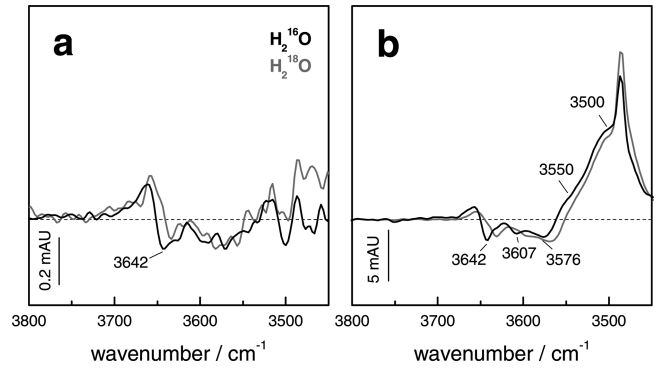

FIGURE 7: Weakly H-bonded O−H region for L-BR. Bands from water O−H stretching vibrations were assigned by their isotopic downshift when $H_2{}^{16}O$ (black lines) was substituted with $H_2{}^{18}O$ (gray lines). (a) Room-temperature L-BR spectrum corrected for the transient heat. (b) Low-temperature L-BR spectrum.

DISCUSSION

Transiently Heated Water and Its Potential Relation with the Photocycle. At room temperature, the earlier spectra in the O−H stretching region are dominated by an intense bilobed peak. This bilobed peak can be effectively reproduced by a static temperature difference spectrum between 298 and 293 K, with a scaling corresponding roughly to an ~0.3 K temperature increase at 2.5 μs. Taking into the account its intensity and how well the bilobe signal is reproduced by the static temperature difference spectrum, we can safely conclude that it originates from the transiently heated sample, mainly from the heated bulk water. Moreover, its intensity is consistent with this interpretation. From the heat capacity of water (1 cal g^{-1} K^{-1}) and considering the heat capacity of bR to be similar to that of soluble proteins (~0.3 cal g^{-1} K^{-1}) (*46*), an ~0.3 K increase of ~800 water molecules and one bR molecule would require an energy of ~0.3 eV. The energy of a 532 nm photon is 2.3 eV, and given the quantum efficiency of the photoisomerization (*47*), the bilobed intensity can be quantitatively explained if the laser pulse initiates the photocycle of ~30% of the bR molecules in the sample, which is quite reasonable given the laser power used in our experiments (*37*). A recent study suggested that the origin of this bilobed peak could lie in the transient heating of ~10 internal water molecules (*20*). This interpretation seems unlikely in view of the shape of the transient heat-induced feature, well explained by heated bulk water. Moreover, if this feature originated from as few as 10 water molecules per bR monomer, it would require an unreasonable transient heating of water molecules from 293 to ~320 K to reproduce the observed bilobed magnitude.

Global exponential fitting of the data in Figure 3a shows that the main L decay and M rise (L-to-M transition) occurs with a time constant of 80 μs, in agreement with previous results at room temperature, and coincident with the observed time constant of the appearance of a proton in the extracelular side in solution (*48, 49*). Under our standard experimental conditions, the decay of the transient heat shows a time constant of ~60 μs, quite similar to those of both the main L-to-M transition and the proton release. An important question is whether the L-to-M transition and the transient heat dissipation of the samples are somehow related (*20*) or, in contrast, whether they are basically uncorrelated processes with accidentally similar time constants (*36*). We

observed that heat relaxation is not affected by the sample temperature (Figure 3b, left panel), whereas it is delayed when the sample thickness increases (Figure 3b, right panel). The dependence on the film thickness and the independence on the sample temperature clearly indicate that, in contrast to a previous suggestion (*20*), the heat relaxation is not related to the L-to-M transition, since this transition is temperature sensitive (*37*), and not affected by the film thickness (see Figure S2 of the Supporting Information). Therefore, the transient thermal heating relaxes as a conventional thermal diffusion process uncorrelated with the photocycle.

Internal Water Molecules in M-BR. The O−H stretching of weakly hydrogen bonded waters has been previously reported above 3550 cm^{-1} for the low-temperature M-BR spectrum (*50*). For the M minus BR spectrum, the bands at 3670 (M), 3642 (BR), 3618 (BR), 3593 (M), and 3569 (M) cm^{-1} can be assigned to water O−H stretching (Figure 5b). Previously, by the use of mutants and correlations with X-ray structures, the 3642, 3593, and 3569 cm^{-1} bands were assigned to O−H vibrations of water molecules close to Asp85 (*38*). Specifically, low-temperature FTIR spectroscopic studies identified the 3643 cm^{-1} band as the O−H stretch of a water molecule (W401) hydrating Asp85 in BR (*51*), where the observed O−H stretch corresponds to the group free from hydrogen bonds. On the other hand, the band at 3669 cm^{-1} was assigned to a water molecule in the cytoplasmic domain in M and the band at 3618 cm^{-1} to a water molecule in the extracellular domain in BR, close to Arg82−Glu204 (*4*). Some of these bands have previously been reported at room temperature. A previous room-temperature study using *in situ* $H_2{}^{16}O-H_2{}^{18}O$ exchange detected a band in BR at 3644 cm^{-1} (*19*), and a time-resolved room-temperature experiment showed two $H_2{}^{18}O$ sensitive bands at 3645 (BR) and 3670 (M) cm^{-1} (*20*), in agreement with the data presented here. Our room-temperature M-BR spectrum shows $H_2{}^{18}O$ sensitive bands at 3668 (M), 3644 (BR), 3620 (BR), 3600 (M), 3580 (M), and 3560 (M) cm^{-1}. Indeed, taking into the account the differences in pH (see Figure S1) and in the signal-to-noise ratio, the M-BR spectra at room (Figure 5a) and low temperature (Figure 5b) reveal very similar changes in the weakly H-bonded O−H stretching region of waters.

It is known that as the H-bond strength increases the O−H vibration frequency decreases, and at the same time, the initially narrow bands develop into very broad bands, making them difficult to detect (*5*). Because of the practical convenience, the O−H stretching of strongly H-bonded waters has been mainly studied in D_2O. From the absence of $D_2{}^{18}O$ sensitive bands, it was concluded that strongly D-bonded waters do not change (or effectively compensate) their D-bonding strength from the BR ground state to M (*41*). Likewise, we did not observe any band shifting in $H_2{}^{18}O$ either at room temperature or at low temperatures, supporting the published results in D_2O. Moreover, the spectral shape in this region is remarkably similar between our low- and room-temperature spectra, giving further support for the equivalence of room- and low-temperature M-BR spectra. Unexpectedly, previous room-temperature M-BR data in this region published by Garczarek and Gerwert (*19*), although with the bands at similar positions and with similar shapes, significantly differ from our data in the baseline [compare our Figure 5c, Figure 5d, and Figure S1 with Figure 2d (blue) of Garczarek and Gerwert (*19*)]. They concluded that new strong H-bonds from waters are formed in M, possibly from waters involved in the proton release group after the proton is released. However, our data do not support any difference in the number of strongly H-bonded waters between M and BR, either at room temperature or at low temperatures.

Besides bands from weakly and strongly H-bonded waters, another spectral signature related to internal water molecules has been reported in the bR photocycle, a continuum band that can be observed at 2200–1700 cm^{-1}, assigned to the deprotonation of a protonated water cluster when a proton is released to the extracellular side in the formation of the M state (*18, 36, 42*). This continuum band is clearly observed in our room-temperature M-BR spectrum (Figure 5e) but not at low temperatures (see Figure 5f and its inset) and represents the main (and basically unique) spectral difference between room- and low-temperature M-BR.

We can conclude that, except from the continuum band, IR changes in internal waters between BR and M states are preserved at 230 K, suggesting that the location of water and interactions in the BR and M states are mostly preserved at 230 K.

Protein Dynamics and Differences between Room- and Low-Temperature M-BR. Our experimental data strongly suggest that at low temperatures (230 K) all the changes involved in the L-to-M transition take place as at room temperature, except from the proton release to the extracellular side, which is inhibited. It seems that at 230 K the thermal energy and/or protein fluctuations are insufficient for this step to take place, as further suggested by the presence of a dynamic transition in BR at ∼250 K (*15*). Moreover, the magnitude of this dynamic transition seems to depend on the dynamics of the water solvating BR (*14, 15, 52*), which could be essential for the release of the proton to take place. When warmed to ∼250 K, the low-temperature M form evolves thermally to N (*53*), so the proton release should take place once the thermal energy or protein dynamics reaches a suitable threshold.

Internal Water Molecules in L-BR. The O−H stretching of weakly hydrogen bonded waters for the low-temperature L-BR spectrum has been reported and studied above 3450 cm^{-1} (*54, 55*). In agreement with previous studies, we also observed five $H_2{}^{18}O$ sensitive bands and two insensitive ones (3486 and 3657 cm^{-1}). As in M-BR, the band at 3642 cm^{-1} is assigned to a water molecule (Wat401) close to Asp85 in BR (*51*). The bands at 3500 (L), 3550 (L), 3576 (BR), and 3607 (BR) cm^{-1} have been assigned by the use of mutants to changes in water molecules located in the cytoplasmic domain differing between L and BR, likely close to Thr46 (*4, 38*), with the band at 3500 cm^{-1} remarkably intense and broad. For room-temperature L-BR, we could assign to water only the band at 3642 (BR) cm^{-1}. Two negative small bands were observed at 3593 and 3571 cm^{-1}, which seem to correlate with the two negative bands observed at low temperatures at 3607 and 3576 cm^{-1}. However, their low intensity combined with the limited signal-to-noise data in $H_2{}^{18}O$ prevented their clear assignment to water.

The more remarkable difference between room- and low-temperature L-BR is the lack of any intense positive broadband at 3500 cm^{-1}. The origin of this intense and broad vibrational band seems to lay in the formation of a structure

of waters connecting the SB and the Thr46−Asp96 region in L, which have been proposed as a requirement for formation and stabilization of the L intermediate (*38, 45*). The possibility that this band is still present at room temperature but is red-shifted seems very unlikely in view of Figure 6b, which does not give any evidence of a positive intense band present at room temperature but not at low temperatures bellow 3400 cm^{-1}. It could be still possible that the band appears at room temperature but is significantly decreased in intensity due to the involvement of fewer water molecules in the cavity at room temperature. In this regard, it is interesting to point out the presence of a new positive band at 3520 cm^{-1} at room temperature, not observed at low temperatures (Figure 6b). Unfortunately, this band does not shift in D_2O (unpublished results), in contrast to the 3500 cm^{-1} band (*56*), so its assignment to water is unlikely. A final possibility is that this band retains its area but becomes broader at room temperature (and so decreases in intensity). The broadening at room temperature could originate from H-bonding strength with a very large variability, with its origin in very fast dynamical fluctuations of the water H-bond strength. However, there is not any apparent positive broadband or positive baseline-like contribution present at room temperature or at low temperatures in the whole O−H stretching region of L-BR, suggesting that the broadening, if present, should be unreasonably large. Moreover, the room-temperature water bands in M-BR are clearly observed, with a bandwidth only slightly higher than that at low temperatures, showing that at room temperature internal water bands do not necessary suffer from extra inhomogeneous broadening caused by faster fluctuations. All this evidence strongly suggests that the presence of the 3500 cm^{-1} band in the low-temperature L-BR spectrum is an artifact caused by the low temperature of the sample. This in turn implies that the conclusions about water changes in the cytoplasmic domain upon formation of the L intermediate, based on the observation of this band at low temperatures, may not be relevant at physiological temperatures. It is also raises reasonable doubts about the actual significance of changes in internal water between L and BR observed in some X-ray crystallographic structures (*57*).

There has been some controversy about discrepancies between low- and room-temperature FTIR data for the strongly H-bonded water region in L. Initially, low-temperature studies in $D_2{}^{16}O$ and $D_2{}^{18}O$ concluded from spectral shifts that at least one strongly H-bonded water present in BR was absent in K and again restored in the L intermediate (*41*). In contrast, room-temperature experiments in H_2O concluded from baseline intensity changes below 3000 cm^{-1} that the strongly H-bonded waters lost in K are not yet restored in the L intermediate (*19*). Since we could not obtain room-temperature L-BR spectra in $H_2{}^{16}O$ and $H_2{}^{18}O$ with sufficient quality, we could not use the method used by Tanimoto et al. (*41*), but only the method used by Garczarek and Gerwert (*19*). Our room-temperature L-BR spectrum corrected for the transient heat (Figure 6b, orange line) shows a baseline-like intensity in the <3000 cm^{-1} region higher than that for the low-temperature L-BR spectrum (Figure 6b, blue), but similar to that of the low-temperature K-BR spectrum (Figure 6b, gray). This result seems to corroborate previous conclusions of Garczarek and Gerwert. However, it is not clear if both experimental approaches (detecting shifts in isotopically labeled water and detecting changes in the baseline intensity) are completely comparable. Specifically, monitoring the baseline seems more prone to artifacts caused by overlapping contributions than detecting an isotopic shift. It seems that further room temperature experiments in D_2O should be performed, ideally in both $D_2{}^{16}O$ and $D_2{}^{18}O$, for more conclusive results.

Protein Dynamics and Differences between Room- and Low-Temperature L-BR. According to IR spectroscopy, the room-temperature protein structure and retinal conformation seem to be basically preserved at 170 K, in spite of some significant differences in the retinal HOOP bands. More important are the observed alterations in bands from internal water molecules. It is interesting to note that bR in purple membranes shows a dynamic transition around 170 K, corresponding to the inhibition of some slow−large motions on the scale of neutron diffraction experiments (*15, 16*). This transition is independent of the sample hydration, and therefore, it seems to be deeply connected to the inhibition of some internal protein motions. The evidence that the observed alterations in the low-temperature L may be connected with this dynamic transition comes from the fact that when warmed to 180 K, low-temperature L goes unproductively back to BR (*53*). In contrast, when warmed from 170 to 220 K, some fraction of L is observed to evolve to M (*53*). It could be possible that only above 200 K could the L intermediate conformation and/or dynamics allow for an internal water disposition compatible for an L-to-M transition. In agreement with this interpretation, it is interesting to note that the pure L-BR spectrum obtained at 220 K and pH 6, using the M back-photoreaction, shows spectral features in the protonated carboxylic region similar to those of the room-temperature L-BR spectrum and significantly different from those of the L-BR spectrum obtained at 170 K (*58*).

ACKNOWLEDGMENT

We are grateful to Leonid Brown for critically reading the manuscript and to Mikihiro Shibata for preparing the purple membrane used in the experiments.

SUPPORTING INFORMATION AVAILABLE

Spectral comparison of the room- and low-temperature M-BR spectra (Figure S1) and decay kinetics of the L intermediate for bR films with different thicknesses (Figure S2). This material is available free of charge via the Internet at http://pubs.acs.org.

REFERENCES

1. Lanyi, J. K. (2004) Bacteriorhodopsin. *Annu. Rev. Physiol. 66*, 665–688.
2. Haupts, U., Tittor, J., and Oesterhelt, D. (1999) Closing in on bacteriorhodopsin: Progress in understanding the molecule. *Annu. Rev. Biophys. Biomol. Struct. 28*, 367–399.
3. Stoeckenius, W. (1999) Bacterial rhodopsins: Evolution of a mechanistic model for the ion pumps. *Protein Sci. 8*, 447–459.
4. Kandori, H. (2000) Role of internal water molecules in bacteriorhodopsin. *Biochim. Biophys. Acta 1460*, 177–191.
5. Kandori, H. (2004) Hydration switch model for the proton transfer in the Schiff base region of bacteriorhodopsin. *Biochim. Biophys. Acta 1658*, 72–79.
6. Luecke, H., Schobert, B., Richter, H. T., Cartailler, J. P., and Lanyi, J. K. (1999) Structure of bacteriorhodopsin at 1.55 Å resolution. *J. Mol. Biol. 291*, 899–911.

7. Belrhali, H., Nollert, P., Royant, A., Menzel, C., Rosenbusch, J. P., Landau, E. M., and Pebay-Peyroula, E. (1999) Protein, lipid and water organization in bacteriorhodopsin crystals: A molecular view of the purple membrane at 1.9 Å resolution. *Structure 7*, 909–917.
8. Luecke, H. (2000) Atomic resolution structures of bacteriorhodopsin photocycle intermediates: The role of discrete water molecules in the function of this light-driven ion pump. *Biochim. Biophys. Acta 1460*, 133–156.
9. Neutze, R., Pebay-Peyroula, E., Edman, K., Royant, A., Navarro, J., and Landau, E. M. (2002) Bacteriorhodopsin: A high-resolution structural view of vectorial proton transport. *Biochim. Biophys. Acta 1565*, 144–167.
10. Lanyi, J. K. (2004) X-ray diffraction of bacteriorhodopsin photocycle intermediates. *Mol. Membr. Biol. 21*, 143–150.
11. Lanyi, J. K. (2004) What is the real crystallographic structure of the L photointermediate of bacteriorhodopsin? *Biochim. Biophys. Acta 1658*, 14–22.
12. Zaccai, G. (2000) How soft is a protein? A protein dynamics force constant measured by neutron scattering. *Science 288*, 1604–1607.
13. Ferrand, M., Dianoux, A. J., Petry, W., and Zaccaï, G. (1993) Thermal motions and function of bacteriorhodopsin in purple membranes: Effects of temperature and hydration studied by neutron scattering. *Proc. Natl. Acad. Sci. U.S.A. 90*, 9668–9672.
14. Lechner, R. E., Fitter, J., Dencher, N. A., and Hauss, T. (1998) Dehydration of biological membranes by cooling: An investigation on the purple membrane. *J. Mol. Biol. 277*, 593–603.
15. Lehnert, U., Réat, V., Weik, M., Zaccaï, G., and Pfister, C. (1998) Thermal motions in bacteriorhodopsin at different hydration levels studied by neutron scattering: Correlation with kinetics and light-induced conformational changes. *Biophys. J. 75*, 1945–1952.
16. Heberle, J., Fitter, J., Sass, H. J., and Büldt, G. (2000) Bacteriorhodopsin: The functional details of a molecular machine are being resolved. *Biophys. Chem. 85*, 229–248.
17. Wang, J., and El-Sayed, M. A. (2001) Time-resolved Fourier transform infrared spectroscopy of the polarizable proton continua and the proton pump mechanism of bacteriorhodopsin. *Biophys. J. 80*, 961–971.
18. Garczarek, F., Brown, L. S., Lanyi, J. K., and Gerwert, K. (2005) Proton binding within a membrane protein by a protonated water cluster. *Proc. Natl. Acad. Sci. U.S.A. 102*, 3633–3638.
19. Garczarek, F., and Gerwert, K. (2006) Functional waters in intraprotein proton transfer monitored by FTIR difference spectroscopy. *Nature 439*, 109–112.
20. Morgan, J. E., Vakkasoglu, A. S., Gennis, R. B., and Maeda, A. (2007) Water Structural Changes in the L and M Photocycle Intermediates of Bacteriorhodopsin as Revealed by Time-Resolved Step-Scan Fourier Transform Infrared (FTIR) Spectroscopy. *Biochemistry 46*, 2787–2796.
21. Noguchi, T., and Sugiura, M. (2002) Flash-induced FTIR difference spectra of the water oxidizing complex in moderately hydrated photosystem II core films: Effect of hydration extent on S-state transitions. *Biochemistry 41*, 2322–2330.
22. Bertie, J. E., and Ahmed, M. K. (1989) Infrared intensities of liquids. 5. Optical and dielectric constants, integrated intensities, and dipole moment derivaties of H_2O and D_2O at 22 °C. *J. Phys. Chem. 93*, 2210–2218.
23. Rahmelow, K., Hübner, W., and Ackermann, T. (1998) Infrared absorbances of protein side chains. *Anal. Biochem. 257*, 1–11.
24. Váró, G., and Lanyi, J. K. (1991) Distortions in the photocycle of bacteriorhodopsin at moderate dehydration. *Biophys. J. 59*, 313–322.
25. Dioumaev, A. K., and Braiman, M. S. (1997) Two bathointermediates of the bacteriorhodopsin photocycle, distinguished by nanosecond time-resolved FTIR spectroscopy at room temperature. *J. Phys. Chem. B 101*, 1655–1662.
26. Hessling, B., Souvignier, G., and Gerwert, K. (1993) A model-independent approach to assigning bacteriorhodopsin's intramolecular reactions to photocycle intermediates. *Biophys. J. 65*, 1929–1941.
27. Zscherp, C., and Heberle, J. (1997) Infrared difference spectra of the intermediates L, M, N, and O of the bacteriorhodopsin photoreaction obtained by time-resolved attenuated total reflection spectroscopy. *J. Phys. Chem. B 101*, 10542–10547.
28. Lórenz-Fonfría, V. A., and Kandori, H. (2007) Bayesian maximum entropy (2D) lifetime distribution reconstruction from time-resolved spectroscopic data. *Appl. Spectrosc. 61*, 428–443.
29. Uhmann, W., Becker, A., Taran, C., and Siebert, F. (1991) Time-resolved FT-IR absorption spectroscopy using a step-scan interferometer. *Appl. Spectrosc. 45*, 390–397.
30. Sasaki, J., Maeda, A., Kato, C., and Hamaguchi, H. (1993) Time-resolved infrared spectral analysis of the KL-to-L conversion in the photocycle of bacteriorhodopsin. *Biochemistry 32*, 867–871.
31. Heberle, J., and Zscherp, C. (1996) ATR/FT-IR difference spectroscopy of biological matter with microsecond time resolution. *Appl. Spectrosc. 50*, 588–596.
32. Rödig, C., Chizhov, I., Weidlich, O., and Siebert, F. (1999) Time-resolved step-scan Fourier transform infrared spectroscopy reveals differences between early and late M intermediates of bacteriorhodopsin. *Biophys. J. 76*, 2687–2701.
33. Maeda, A. (1995) Application of FTIR spectroscopy to the structural study on the function of bacteriorhodopsin. *Isr. J. Chem. 35*, 387–400.
34. Dioumaev, A. K. (2001) Infrared methods for monitoring the protonation state of carboxylic amino acids in the photocycle of bacteriorhodopsin. *Biochemistry (Moscow) 66*, 1269–1276.
35. Perálvarez-Marín, A., Lórenz-Fonfría, V. A., Bourdelande, J.-L., Querol, E., Kandori, H., and Padrós, E. (2007) Inter-helical hydrogen bonds are essential elements for intra-protein signal transduction: The role of Asp115 in bacteriorhodopsin transport function. *J. Mol. Biol. 368*, 666–676.
36. Garczarek, F., Wang, J., El-Sayed, M. A., and Gerwert, K. (2004) The assignment of the different infrared continuum absorbance changes observed in the 3000–1800-cm^{-1} region during the bacteriorhodopsin photocycle. *Biophys. J. 87*, 2676–2682.
37. Chizhov, I., Chernavskii, D. S., Engelhard, M., Mueller, K. H., Zubov, B. V., and Hess, B. (1996) Spectrally silent transitions in the bacteriorhodopsin photocycle. *Biophys. J. 71*, 2329–2345.
38. Maeda, A. (2001) Internal water molecules as mobile polar groups for light-induced proton translocation in bacteriorhodopsin and rhodopsin as studied by difference FTIR spectroscopy. *Biochemistry (Moscow) 66*, 1256–1268.
39. Kandori, H., Kinoshita, N., Shichida, Y., and Maeda, A. (1998) Protein structural changes in bacteriorhodopsin upon photoisomerization as revealed by polarized FTIR spectroscopy. *J. Phys. Chem. B 102*, 7899–7905.
40. Kandori, H., Kinoshita, N., Yamazaki, Y., Maeda, A., Shichida, Y., Needleman, R., Lanyi, J. K., Bizounok, M., Herzfeld, J., Raap, J., and Lugtenburg, J. (2000) Local and distant protein structural changes on photoisomerization of the retinal in bacteriorhodopsin. *Proc. Natl. Acad. Sci. U.S.A. 97*, 4643–4648.
41. Tanimoto, T., Furutani, Y., and Kandori, H. (2003) Structural changes of water in the Schiff base region of bacteriorhodopsin: Proposal of a hydration switch model. *Biochemistry 42*, 2300–2306.
42. Rammelsberg, R., Huhn, G., Lübben, M., and Gerwert, K. (1998) Bacteriorhodopsin's intramolecular proton-release pathway consists of a hydrogen-bonded network. *Biochemistry 37*, 5001–5009.
43. Lanyi, J. K. (2006) Proton transfers in the bacteriorhodopsin photocycle. *Biochim. Biophys. Acta 1757*, 1012–1018.
44. Weidlich, O., and Siebert, F. (1993) Time-resolved step-scan FT-IR investigations of the transition from KL to L in the bacteriorhodopsin photocycle: Identification of chromophore twists by assigning hydrogen-out-of-plane (HOOP) bending vibrations. *Appl. Spectrosc. 47*, 1394–1399.
45. Maeda, A., Morgan, J. E., Gennis, R. B., and Ebrey, T. G. (2006) Water as a cofactor in the unidirectional light-driven proton transfer steps in bacteriorhodopsin. *Photochem. Photobiol. 82*, 1398–1405.
46. Gómez, J., Hilser, V. J., Xie, D., and Freire, E. (1995) The heat capacity of proteins. *Proteins 22*, 404–412.
47. Tittor, J., and Oesterhelt, D. (1990) The quantum yield of becteriorhodopsin. *FEBS Lett. 263*, 269–273.
48. Alexiev, U., Mollaaghababa, R., Scherrer, P., Khorana, H. G., and Heyn, M. P. (1995) Rapid long-range proton diffusion along the surface of the purple membrane and delayed proton transfer into the bulk. *Proc. Natl. Acad. Sci. U.S.A. 92*, 372–376.
49. Heberle, J., and Dencher, N. A. (1990) Bacteriorhodopsin in ice. Accelerated proton transfer from the purple membrane surface. *FEBS Lett. 277*, 277–280.
50. Yamazaki, Y., Kandori, H., Needleman, R., Lanyi, J. K., and Maeda, A. (1998) Interaction of the protonated Schiff base with the peptide backbone of valine 49 and the intervening water molecule in the N photointermediate of bacteriorhodopsin. *Biochemistry 37*, 1559–1564.
51. Shibata, M., and Kandori, H. (2005) FTIR studies of internal water molecules in the Schiff base region of bacteriorhodopsin. *Biochemistry 44*, 7406–7413.
52. Weik, M. (2003) Low-temperature behavior of water confined by biological macromolecules and its relation to protein dynamics. *Eur. Phys. J. E 12*, 153–158.

53. Balashov, S. P., and Ebrey, T. G. (2001) Trapping and spectroscopic identification of the photointermediates of bacteriorhodopsin at low temperatures. *Photochem. Photobiol. 73*, 453–462.
54. Yamazaki, Y., Hatanaka, M., Kandori, H., Sasaki, J., Karstens, W. F., Raap, J., Lugtenburg, J., Bizounok, M., Herzfeld, J., Needleman, R., Lanyi, J. K., and Maeda, A. (1995) Water structural changes at the proton uptake site (the Thr46-Asp96 domain) in the L intermediate of bacteriorhodopsin. *Biochemistry 34*, 7088–7093.
55. Yamazaki, Y., Tuzi, S., Saito, H., Kandori, H., Needleman, R., Lanyi, J. K., and Maeda, A. (1996) Hydrogen bonds of water and C═O groups coordinate long-range structural changes in the L photointermediate of bacteriorhodopsin. *Biochemistry 35*, 4063–4068.
56. Yamazaki, Y., Sasaki, J., Hatanaka, M., Kandori, H., Maeda, A., Needleman, R., Shinada, T., Yoshihara, K., Brown, L. S., and Lanyi, J. K. (1995) Interaction of tryptophan-182 with the retinal 9-methyl group in the L intermediate of bacteriorhodopsin. *Biochemistry 34*, 577–582.
57. Kouyama, T., Nishikawa, T., Tokuhisa, T., and Okumura, H. (2004) Crystal structure of the L intermediate of bacteriorhodopsin: Evidence for vertical translocation of a water molecule during the proton pumping cycle. *J. Mol. Biol. 335*, 531–546.
58. Ormos, P., Chu, K., and Mourant, J. (1992) Infrared study of the L, M, and N intermediates of bacteriorhodopsin using the photoreaction of M. *Biochemistry 31*, 6933–6937.

BI7024063